


Article

# A Calorimetric and Thermodynamic Investigation of the Synthetic Analogue of Mandarinoite, $\text{Fe}_2(\text{SeO}_3)_3 \cdot 5\text{H}_2\text{O}$

Maxim I. Lelet<sup>1</sup>, Marina V. Charykova<sup>2</sup>, Astrid Holzheid<sup>3</sup> , Brendan Ledwig<sup>3</sup>, Vladimir G. Krivovichev<sup>2,\*</sup> and Evgeny V. Suleimanov<sup>1</sup>

<sup>1</sup> Research Institute for Chemistry, Lobachevsky State University of Nizhny Novgorod, Gagarin Ave. 23, Nizhny Novgorod 603950, Russia; maxlelet@gmail.com (M.I.L.); suev@unn.ru (E.V.S.)

<sup>2</sup> Department of Geology, St. Petersburg State University, 7-9 University Embankment, Saint-Petersburg 199034, Russia; m-char@yandex.ru

<sup>3</sup> Institute of Geosciences, Kiel University, 24098 Kiel, Germany; astrid.holzheid@ifg.uni-kiel.de (A.H.); brendan.ledwig@ifg.uni-kiel.de (B.L.)

\* Correspondence: vkrivovi@yandex.ru

Received: 24 August 2018; Accepted: 9 October 2018; Published: 28 October 2018



**Abstract:** Thermophysical and thermochemical calorimetric investigations were carried out on the synthetic analogue of mandarinoite. The low-temperature heat capacity of  $\text{Fe}_2(\text{SeO}_3)_3 \cdot 5\text{H}_2\text{O}(\text{cr})$  was measured using adiabatic calorimetry between 5.3 and 324.8 K, and the third-law entropy was determined. Using these  $C_{p,m}^{\circ}(T)$  data, the third law entropy at  $T = 298.15$  K,  $S_m^{\circ}$ , is calculated as  $520.1 \pm 1.1 \text{ J} \cdot \text{K}^{-1} \cdot \text{mol}^{-1}$ . Smoothed  $C_{p,m}^{\circ}(T)$  values between  $T \rightarrow 0$  K and 320 K are presented, along with values for  $S_m^{\circ}$  and the functions  $[H_m^{\circ}(T) - H_m^{\circ}(0)]$  and  $[\Phi_m^{\circ}(T) - \Phi_m^{\circ}(0)]$ . The enthalpy of formation of  $\text{Fe}_2(\text{SeO}_3)_3 \cdot 5\text{H}_2\text{O}(\text{cr})$  was determined by solution calorimetry with HF solution as the solvent, giving  $\Delta_f H_m^{\circ}(298 \text{ K}, \text{Fe}_2(\text{SeO}_3)_3 \cdot 5\text{H}_2\text{O}, \text{cr}) = -3124.6 \pm 5.3 \text{ kJ/mol}$ . The standard Gibbs energy of formation for  $\text{Fe}_2(\text{SeO}_3)_3 \cdot 5\text{H}_2\text{O}(\text{cr})$  at  $T = 298$  K can be calculated on the basis on  $\Delta_f H_m^{\circ}(298 \text{ K})$  and  $\Delta_f S_m^{\circ}(298 \text{ K})$ :  $\Delta_f G_m^{\circ}(298 \text{ K}, \text{Fe}_2(\text{SeO}_3)_3 \cdot 5\text{H}_2\text{O}, \text{cr}) = -2600.8 \pm 5.4 \text{ kJ/mol}$ . The value of  $\Delta_f G_m^{\circ}$  for  $\text{Fe}_2(\text{SeO}_3)_3 \cdot 5\text{H}_2\text{O}(\text{cr})$  was used to calculate the Eh–pH diagram of the Fe–Se–H<sub>2</sub>O system. This diagram has been constructed for the average contents of these elements in acidic waters of the oxidation zones of sulfide deposits. The behaviors of selenium and iron in the surface environment have been quantitatively explained by variations of the redox potential and the acidity-basicity of the mineral-forming medium. These parameters precisely determine the migration ability of selenium compounds and its precipitation in the form of solid phases.

**Keywords:** mandarinoite; adiabatic calorimetry; heat capacity; entropy; enthalpy of formation; the Gibbs energy of formation

## 1. Introduction

Hydrous selenite minerals are found, as a rule, in the oxidation zone of sulfide and selenide ores [1,2]. Our understanding of low-temperature mineral assemblages strongly depends on our knowledge of the thermodynamic stability of the constituting mineral phases. Experimental and thermodynamic modeling is quite essential to analyze the conditions under which selenites and selenates replace selenides, and selenium-bearing sulfides in the oxidation zones of sulfide ore deposits or upon weathering of technologic waste. The physicochemical modeling is based on the thermodynamic constants of minerals. Reliable solubility product or Gibbs energy of formation values of the phases crystallized in the system are necessary for calculation of mineral equilibria. In this study, we continue our systematic investigation of the thermodynamic properties of hydrous selenites [3–5]

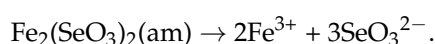
by performing a calorimetric and thermodynamic study of hydrous ferric selenite, a synthetic analogue of mandarinoite,  $(\text{Fe}_2(\text{SeO}_3)_3 \cdot 5\text{H}_2\text{O})$ .

Mandarinoite was found for the first time at Pacajake mine near Hiaco, Colquechaca, Bolivia [6], where it is associated with native selenium, siderite ( $\text{FeCO}_3$ ), penroseite ( $\text{NiSe}_2$ ), and alteration products of selenides and selenium-bearing sulfides such as ahlfeldite ( $\text{NiSeO}_3 \cdot 2\text{H}_2\text{O}$ ), cobaltomenite ( $\text{CoSeO}_3 \cdot 2\text{H}_2\text{O}$ ), chalcomenite ( $\text{CuSeO}_3 \cdot 2\text{H}_2\text{O}$ ), and molybdomenite ( $\text{PbSeO}_3$ ). The water content of mandarinoite was not directly analyzed by Dunn et al. [6], but the amount of water was derived from difference based on electron microprobe analysis ( $\Sigma(\text{Fe}_2\text{O}_3 + \text{SeO}_2) + \text{H}_2\text{O} = 100.00$  wt %) and the theoretical formula of the new mineral was deduced as  $\text{Fe}_2(\text{SeO}_3)_3 \cdot 4\text{H}_2\text{O}$ . A single ferric selenite hydrate crystal from De Lamar silver mine was studied by Hawthorne [7], who derived the ideal formula of mineral  $(\text{Fe}_2(\text{SeO}_3)_3 \cdot 6\text{H}_2\text{O})$  from the structure based on single-crystal X-ray precession photographs. In our recent work [8], based on XRD measurements and thermal analysis, we were able to derive  $\text{Fe}_2(\text{SeO}_3)_3 \cdot (6 - x)\text{H}_2\text{O}$  ( $x = 0.0\text{--}1.0$ ) as the formula of the hydrous ferric selenite mandarinoite. The total amount of water apparently affects the crystallinity, and possibly the stability of crystals: the lower the  $x$  value, the higher crystallinity can be expected. The sample synthesized by us, identical to mandarinoite according to XRD analysis, has the composition  $\text{Fe}_2(\text{SeO}_3)_3 \cdot 5\text{H}_2\text{O}$ .

The analysis of the thermodynamic parameters (solubility product or Gibbs energy of formation) for calculation of mineral equilibria involving selenites [1–3,5,9–11] showed that these parameters frequently raise questions and need specification.

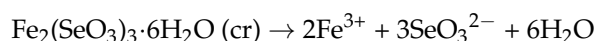
No calorimetric determination of the standard enthalpy of formation of iron(III) selenites from aqueous solution has been found. Chukhlantsev and Tomashevsky [12] were the first to study the solubility of iron(III) selenite with respect to other selenites. The solubility of the specimen in a dilute solution of nitric or sulfuric acid was measured at 293 K. The solid phase, however, was identified only by the determination of Fe and Se concentration and it was assumed that the composition of the solid phase is  $\text{Fe}_2(\text{SeO}_3)_2$ . The reported value of the solubility product is  $(-30.91 \pm 0.25)$  [12]. No information on the quality of the specimen is available but, according to the authors of [10], it is most likely amorphous.

The authors of this book recalculated the data of [12] for the equilibrium:



The result was  $\log_{10}K(293.15 \text{ K}) = (-33.77 \pm 0.15)$ , but it is not selected [10] due to insufficient characteristics of the solid phase.

The value of the solubility product obtained in the study of Rai et al. [13] for  $\text{Fe}_2(\text{SeO}_3)_3 \cdot 6\text{H}_2\text{O}$  is more than 10 orders of magnitude less than that reported value. Their result for the equilibrium:



is  $\log_{10}K(296 \text{ K}) = (-41.58 \pm 0.11)$ , and it is selected in the reference book [10]. This is the value we used earlier [1,2,14] to calculate the Eh-pH diagram in the system Fe-Se- $\text{H}_2\text{O}$ . However, Giester et al. [15] reinvestigated compounds synthesized by the method of Rai et al. [16] and studied the synthetic phases by chemical analysis, IR spectroscopy, powder and single crystal X-ray diffraction as well as thermogravimetric analysis. Giester et al. [15] were able to show that the formula of synthetic analogue of mandarinoite, i.e.,  $\text{Fe}_2(\text{SeO}_3)_3 \cdot 6\text{H}_2\text{O}$ , is erroneous and should be rewritten as  $\text{Fe}_2(\text{SeO}_3)_3 \cdot 3\text{H}_2\text{O}$ . Thus, the value of  $\lg SP$  obtained in the work [13] apparently is not a characteristic value of mandarinoite, but describes the other iron selenite— $\text{Fe}_2(\text{SeO}_3)_3 \cdot 3\text{H}_2\text{O}$ .

It should be noted that the experimental determination of thermodynamic data of rare minerals in general, and of the hydrous ferric selenite mandarinoite in particular, on the basis of studying their solubility or by calorimetric measurements, can hardly rely on natural samples, because these usually do not occur in sufficient amounts, form only tiny crystals, may include inclusions, be covered by weathering crusts, and almost inevitably contain impurities. All these defects influence

many properties of the samples studied and certainly their thermodynamic parameters. In this communication we therefore present the results of our investigations of the enthalpy of formation and of the heat capacity of the synthetic analogue of mandarinoite  $\text{Fe}_2(\text{SeO}_3)_3 \cdot 5\text{H}_2\text{O}$ .

## 2. Experimental Methods

### 2.1. Sample Preparation

Detailed description of synthesis technique of analogues of mandarinoite are given in [8]. In short, powdered  $\text{SeO}_2$  (initial weight:  $\sim 0.207$  g) and  $\text{FeCl}_3 \cdot 6\text{H}_2\text{O}$  ( $\sim 0.331$  g) dissolved in distilled water (26 mL) were mixed together. The purity of the starting materials is given in Table 1. The solutions were placed in Teflon containers (total reactor volume: 55.75 mL), which were then positioned in steel autoclaves. The entire reactors were transferred to Memmert<sup>®</sup> heating ovens at room temperature and heated up to 30 °C, inducing an autogenous pressure of 1.5 bar due to the thermal expansion of the fluid in relation to the filling rate. A synthetic analogue of mandarinoite only formed under low-hydrothermal conditions at 30 °C (see [8] for more details). Pre-run and post-run pH values were more or less constant (pre-run pH  $1.03 \pm 0.02$ ; post-run pH  $1.09 \pm 0.03$ ). The duration of synthesis varied between 34 and 69 days. Synthesis experiments were terminated by removing the autoclaves from the heating oven and immediately opening them. The solid particles were filtered out, desiccated overnight, and stored in an exsiccator until further analysis. Sample recovery was  $254 \pm 25$  mg (except for sample 9 with only 152 mg; please note sample identification is identical to [8]). As precise calorimetric determination requires a fairly large mass (in our study we used  $\sim 500$  mg for determination of heat capacity and 200 to 500 mg for heat of solution determination; see below for more details), synthetic analogues of mandarinoite of various runs (9, 13, 14, 15, 16) were combined and used for calorimetric investigation.

**Table 1.** Characterization of compounds used or synthesized in this study.

Compound	Source	Initial Mass Fraction Purity	Purification Method	Final Mass Fraction Purity	Analysis Method
Selenium(IV) oxide	Alfa Aesar	0.994	None <sup>a</sup>		
Iron(III) chloride·6H <sub>2</sub> O	Alfa Aesar	$\geq 0.97$	None <sup>a</sup>		
Sodium selenate	Vecos	0.998	None <sup>a</sup>		
Sodium nitrate	Vecos	0.998	None <sup>a</sup>		
Iron(III) nitrate nonahydrate	Vecos	0.998	None <sup>a</sup>		
Hydrofluoric acid (45%)	Halopolymer	0.9999	None <sup>a</sup>		
$\text{Fe}_2(\text{SeO}_3)_3 \cdot 5\text{H}_2\text{O}$	Synthetic			0.97	XRD <sup>b</sup> , XRF <sup>bc</sup>

<sup>a</sup> not specified by the supplier. <sup>b</sup> X-ray fluorescence analysis. <sup>c</sup> X-ray powder diffraction.

### 2.2. Calorimetric Methods

Low-temperature heat capacity,  $C_{p,m}^o$ , was determined using adiabatic calorimetry for the temperature range  $T = 5.3$  to 324.8 K for  $\text{Fe}_2(\text{SeO}_3)_3 \cdot 5\text{H}_2\text{O}(\text{cr})$ . Measurements were done using a “AK-9.02/BCT-21”-type calorimeter (TERMAX, Moscow, Russia). The experimental uncertainty was determined from previous heat-capacity measurements made on benzoic acid (mass fraction purity 0.99998) and synthetic sapphire,  $\alpha\text{-Al}_2\text{O}_3$  (mass fraction purity 0.99999). The  $C_{p,m}^o$  results between  $T = 5$  and 330 K on the benzoic acid, compared to published values [17], are shown in Figure S1. The  $C_{p,m}^o$  results between  $T = 5$  and 273 K on the synthetic sapphire, compared to published values [18], are shown in Figure S2. The agreement is better than 0.4% at  $T > 20$  K and 2.0% at  $T < 20$  K for benzoic acid, and better than 0.2% at  $T > 30$  K and 2.0% at  $T < 30$  K for sapphire. We conclude, with this calorimeter and our experimental setup, that  $C_{p,m}^o(T)$  can be determined with a standard deviation of  $\pm 2\%$  for the temperature interval from  $T = 5$  to 15 K,  $\pm 0.5\%$  from  $T = 15$  to 40 K and  $\pm 0.2\%$  from  $T = 40$  to 330 K at the 0.95 level of confidence ( $k = 2$ ).

The heat capacity of  $\text{Fe}_2(\text{SeO}_3)_3 \cdot 5\text{H}_2\text{O}(\text{cr})$  was measured on a powder pressed into pellets with masses of 0.562 g in the first series and 0.555 g in the second series. Liquid nitrogen and helium were used to reach cryogenic temperatures in two different sets of  $C_{p,m}^o(T)$  determinations. One set of data was collected between  $T = 78.7$  to 324.8 K and the other from  $T = 5.2$  to 85.4 K. For the measurements an evacuated titanium ampoule, which was closed and hermetically sealed using indium after adding a sample pellet, was filled with dry helium to serve as a heat exchanger (room temperature and 0.008 MPa pressure). Further details on the construction of the calorimeter and the experimental procedures are given in [19].

The  $\Delta_f H_m^o$  (298 K, 0.1 MPa) for  $\text{Fe}_2(\text{SeO}_3)_3 \cdot 5\text{H}_2\text{O}(\text{cr})$  was determined using the heat of solution calorimetry with HF as the solvent. The experiments were performed in a differential heat-conducting Tian–Calvet calorimeter operating at  $T = 298$  K [20]. Dissolution experiments on ground powders were performed inside a large outer Teflon container that, in turn, holds a smaller inner Teflon vessel. The inner vessel contains the sample and the external container the solvent (volume 25 mL) consisting of 8.5 M hydrofluoric acid. The acid:sample ratio was chosen to fully dissolve a solid sample having a mass between 200 and 500 mg within 5 to 10 min. The solution was stirred by a solvent-air mixing system integrated into the calorimeter in order to aid the dissolution process. The enthalpy for the dissolution of potassium chloride (mass fraction purity 0.9998) in doubly distilled and deionized water was measured (molar ratio  $\text{KCl}:\text{H}_2\text{O} = 1:200$ ) in order to determine the precision of the calorimeter and our experimental methodology. Seven experiments were performed and an average value of  $\Delta_{\text{sol}} H_m^o = 17.49 \pm 0.51 \text{ kJ} \cdot \text{mol}^{-1}$  was obtained, which agrees well with the value from the literature of  $17.56 \pm 0.08 \text{ kJ} \cdot \text{mol}^{-1}$  [21]. The statistical Student's *t*-distribution was below 3% for the whole experimental series.

The iron(III) nitrate used for HF-solution calorimetry was in its nonahydrate form  $\text{Fe}(\text{NO}_3)_3 \cdot 9\text{H}_2\text{O}(\text{cr})$ . The compound was purchased newly for these experiments, and the package was unopened until the initiation of the experiments. To avoid hygroscopic reactions, the reagent was stored in a tightly closed reagent bottle and all manipulations were performed in a laboratory maintained at low humidity (<20%). To test the potential for hygroscopicity during routine manipulations, a 0.3 g control sample was open to the air for 1 h. The mass of the sample actually decreased slightly (0.002 g), confirming the slow dehydration of nonahydrate of iron(III) nitrate in the open air to a form of hexahydrate of iron(III) nitrate described in the literature [22]. The sample used for the experiment was in the open air (air humidity <20%) only during weighing (not more than 3 min). After weighing, the sample was immediately placed in a tightly closed reaction vial with small volume, precluding contact with air [20].

### 3. Results

#### 3.1. Sample Characterization

Synthetic analogues of mandarinoite were optically inspected by scanning electron microscopy (SEM) and characterized by X-ray diffractometry. Figure 1 illustrates the optical appearance of synthetic analogues of mandarinoite.

The chemical composition of solid phases was measured using energy dispersive X-ray microanalysis. The average Se:Fe ratio of 1:1.52 for synthetic analogues of mandarinoite corresponds to the stoichiometric ratio Se:Fe equal to 3:2. The amounts of other elements were below the detection limit, with the exception of some samples with traces of Cl, which apparently remained after synthesis with ferric chloride. A small amount of Cl (less than 0.2%) was detected in samples #10 and #11 [8]. As those samples consist of both ferric selenite hydrates,  $\text{Fe}_2(\text{SeO}_3)_3 \cdot 3\text{H}_2\text{O}$  and  $\text{Fe}_2(\text{SeO}_3)_3 \cdot 5\text{H}_2\text{O}$ , the samples were not further studied regarding the calorimetric and thermodynamic investigation.

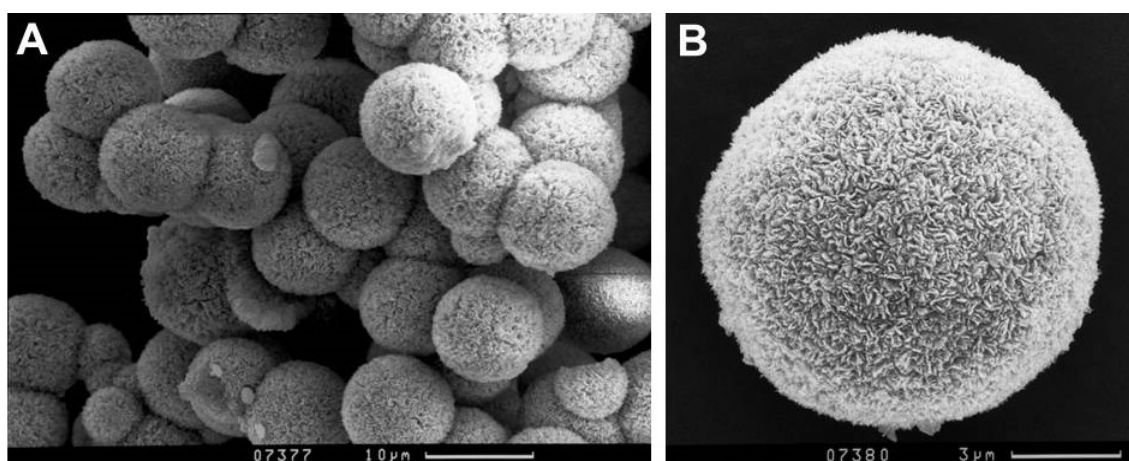


**Figure 1.** Secondary electron images of representative synthetic analogue of mandarinoite (sample #9; 30 °C, 1.5 bar, 47 days).

The X-ray powder diffraction (XRD) patterns clearly indicate that synthesized solid phases are synthetic analogues of mandarinoite (Figure 2). The unit-cell parameters calculated from the powder data are in good accordance with data obtained by other authors for natural mandarinoite (Table 2).

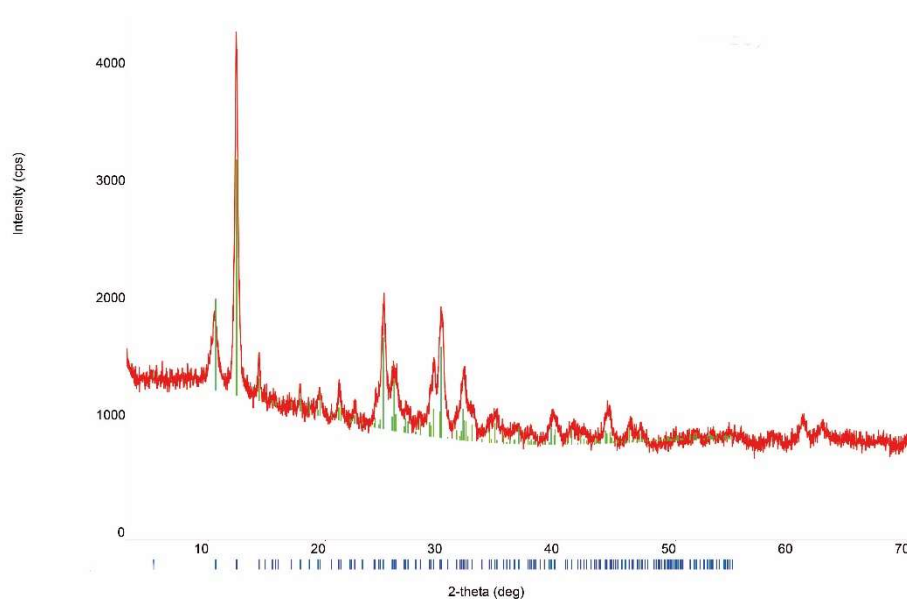


**Figure 2.** Representative XRD patterns of synthetic analogue of mandarinoite (sample #9; 30 °C, 1.5 bar, 47 days) [8]. The blue bars depict the theoretical XRD reflexes of mandarinoite.

**Table 2.** Cell parameters of mandarinoite (Space group  $P2_1/c$ ).

Cell Parameters	Mandarinoite $\text{Fe}_2(\text{SeO}_3)_3 \cdot 4\text{H}_2\text{O}$	Mandarinoite $\text{Fe}_2(\text{SeO}_3)_3 \cdot 6\text{H}_2\text{O}$	Synthetic Analogue of Mandarinoite #9	Synthetic Analogue of Mandarinoite #16
$a$ , Å	16.78(3)	16.810(4)	16.824(6)	16.771(13)
$b$ , Å	7.86(1)	7.880(2)	7.849(3)	7.825(5)
$c$ , Å	9.96(6)	10.019(2)	10.010(4)	10.008(6)
$\beta$ , °	98.3(6)	98.26(2)	98.20(2)	98.21(4)
$V$ , Å <sup>3</sup>		1313(4)	1308(2)	1300(1)
Source	[6]	[7]	[8]	This work



The amount of water and the thermal behavior of the synthesized phases were investigated by thermal analysis with thermogravimetry, difference thermogravimetry, and differential scanning calorimetry. The released volatile phases were determined by thermogravimetric analyses combined with mass spectrometry.

Representative measurements of thermal behavior of synthetic analogue of mandarinoite are illustrated in Figure 3 (TG, DTG, DSC curves). Measurements were performed under air with heating ramps of 5 K/min.

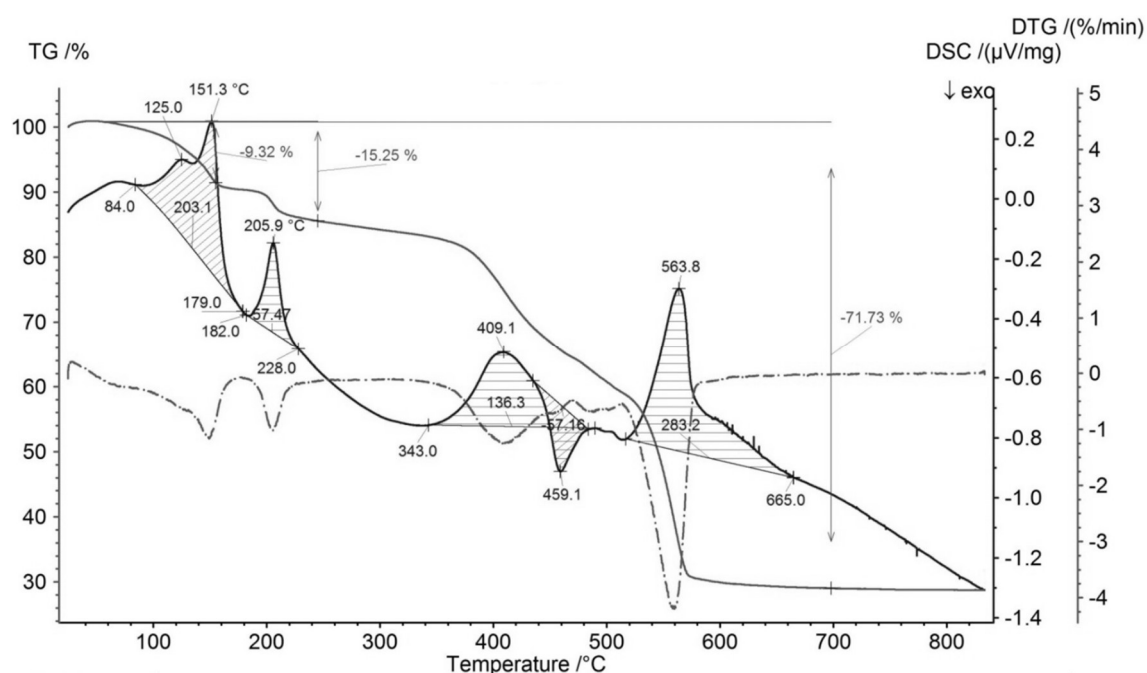


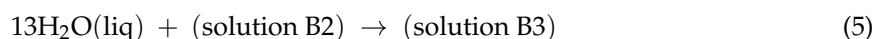
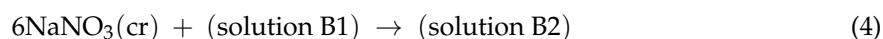
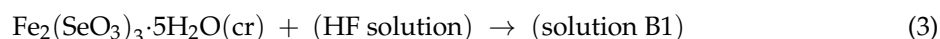
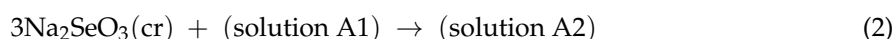
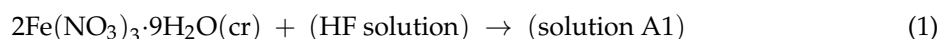
**Figure 3.** TG, DTG and DSC curves of synthesized analogue of mandarinoite (sample #9; 30 °C, 1.5 bar, 47 days) [8]. TG (gray solid line), DSC (black solid line), DTG (gray dashed line).

From Figure 3, within the temperature range 25–300 °C, there are two endothermic effects accompanied by mass losses. These effects occur in the temperature intervals 84–179 °C and 182–228 °C, respectively. The total mass loss of these two effects is 15.25 wt %, which coincides with the calculated value of mass loss of the dehydration reaction of ferric selenite hydrates with five molecules of water, i.e.,  $\text{Fe}_2(\text{SeO}_3)_3 \cdot 5\text{H}_2\text{O} \rightarrow \text{Fe}_2(\text{SeO}_3)_3 + 5\text{H}_2\text{O}$  (15.4 wt %). Thus, the synthesized ferric selenite hydrate contains five molecules of water.

More detailed information regarding the sample characterization is provided by Holzheid et al. [8].

### 3.2. Enthalpy of Formation

The determination of the standard enthalpy of formation,  $\Delta_f H_m^\circ(298 \text{ K})$ , for  $\text{Fe}_2(\text{SeO}_3)_3 \cdot 5\text{H}_2\text{O}(\text{cr})$  was performed using HF solution calorimetry. In order to do so, the enthalpy of solution at  $T = 298 \text{ K}$  was determined for each of the following phases:



The respective values are given in Table 3. Writing the reaction



**Table 3.** Enthalpy of solution values for reactions (1) to (5) at  $T = 298 \text{ K}$  and  $p = 0.1 \text{ MPa}$  <sup>a</sup>.

No.	Reaction	$\Delta_r H_m^\circ / \text{kJ} \cdot \text{mol}^{-1}$
(1)	$2\text{Fe}(\text{NO}_3)_3 \cdot 9\text{H}_2\text{O}(\text{cr}) + (\text{HF solution}) \rightarrow (\text{solution A1})$	33.52
		33.56
		32.54
		33.00
		32.28
		Mean $32.98 \pm 0.71$
(2)	$3\text{Na}_2\text{SeO}_3(\text{cr}) + (\text{solution A1}) \rightarrow (\text{solution A2})$	−131.25
		−127.35
		−123.09
		−130.68
		−134.25
Mean $−129.32 \pm 4.90$		
(3)	$\text{Fe}_2(\text{SeO}_3)_3 \cdot 5\text{H}_2\text{O}(\text{cr}) + (\text{HF solution}) \rightarrow (\text{solution B1})$	5.16
		5.43
		5.66
		5.24
		Mean $5.37 \pm 0.35$
(4)	$6\text{NaNO}_3(\text{cr}) + (\text{solution B1}) \rightarrow (\text{solution B2})$	110.10
		108.60
		108.60
		109.50
		106.56
Mean $108.67 \pm 1.67$		
(5)	$13\text{H}_2\text{O}(\text{liq}) + (\text{solution B2}) \rightarrow (\text{solution B3})$	−9.23
		−8.45
		−10.14
		−10.27
		−8.71
		−9.75
		−10.01
		−9.10
		−9.49
		−8.84
−8.84		
Mean $−9.35 \pm 0.42$		

<sup>a</sup> Standard uncertainty,  $u$ , is  $u(T) = 0.1 \text{ K}$  and  $u(p) = 0.001 \text{ MPa}$ . The expanded uncertainties for  $\Delta H$  are given with a 0.95 level of confidence ( $k \approx 2$ ).

Following Hess' law, one obtains:

$$\Delta_r H_6^\circ(298 \text{ K}) = \Delta_r H_1^\circ(298 \text{ K}) + \Delta_r H_2^\circ(298 \text{ K}) - \Delta_r H_3^\circ(298 \text{ K}) - \Delta_r H_4^\circ(298 \text{ K}) - \Delta_r H_5^\circ(298 \text{ K}) \quad (7)$$

and

$$\Delta_f H_m^\circ(298 \text{ K}, \text{Fe}_2(\text{SeO}_3)_3 \cdot 5\text{H}_2\text{O}, \text{cr}) = \Delta_r H_6^\circ(298 \text{ K}) + 2\Delta_f H_m^\circ(298 \text{ K}, \text{Fe}(\text{NO}_3)_3 \cdot 9\text{H}_2\text{O}, \text{cr}) + 3\Delta_f H_m^\circ(298 \text{ K}, \text{Na}_2\text{SeO}_3, \text{cr}) - 6\Delta_f H_m^\circ(298 \text{ K}, \text{NaNO}_3, \text{cr}) - 13\Delta_f H_m^\circ(298 \text{ K}, \text{H}_2\text{O}, \text{liq}). \quad (8)$$

From the experimental results in Table 3 and the literature data [23], namely  $\Delta_f H_m^\circ(298 \text{ K}, \text{Fe}(\text{NO}_3)_3 \cdot 9\text{H}_2\text{O}, \text{cr}) = -3285.3 \text{ kJ/mol}$ ,  $\Delta_f H_m^\circ(298 \text{ K}, \text{Na}_2\text{SeO}_3, \text{cr}) = -958.6 \text{ kJ/mol}$ ,  $\Delta_f H_m^\circ(298 \text{ K},$

$\text{NaNO}_3, \text{cr}) = -467.85 \text{ kJ/mol}$ ,  $\Delta_f H_m^\circ(298 \text{ K}, \text{H}_2\text{O}, \text{liq}) = -285.83 \text{ kJ/mol}$ , one obtains  $\Delta_f H_m^\circ(298 \text{ K}, \text{Fe}_2(\text{SeO}_3)_3 \cdot 5\text{H}_2\text{O}, \text{cr}) = -3124.6 \pm 5.3 \text{ kJ/mol}$ .

### 3.3. Heat-Capacity Behavior

The raw low-temperature molar heat capacity ( $C_{p,m}^\circ(T)$ ) data for the  $\text{Fe}_2(\text{SeO}_3)_3 \cdot 5\text{H}_2\text{O}(\text{cr})$  are given in the Supplementary Materials (see Table S3). Figure 4 presents the temperature dependence of mandarinoite (cr) heat capacity in the temperature range  $T = 5.2$  to  $324.8 \text{ K}$ . The ferric selenite hydrate  $\text{Fe}_2(\text{SeO}_3)_3 \cdot 5\text{H}_2\text{O}(\text{cr})$  undergoes one phase transition within the temperature range studied. The observed endothermic transition is reversible, and was reproduced by repeated cooling and heating. The maximum of the heat capacity of the sample in the transition range  $T = 21$  to  $45 \text{ K}$  corresponds to a phase transition temperature of  $T_{\text{tr}} = 33.4 \text{ K}$ . The enthalpy of transition  $\Delta_{\text{tr}} H_m^\circ = 123.4 \text{ J/mol}$  was calculated by subtracting the integral computed from the interpolated heat capacities in the transition range from that computed from the measured  $C_{p,m}^\circ(T)$  of mandarinoite.

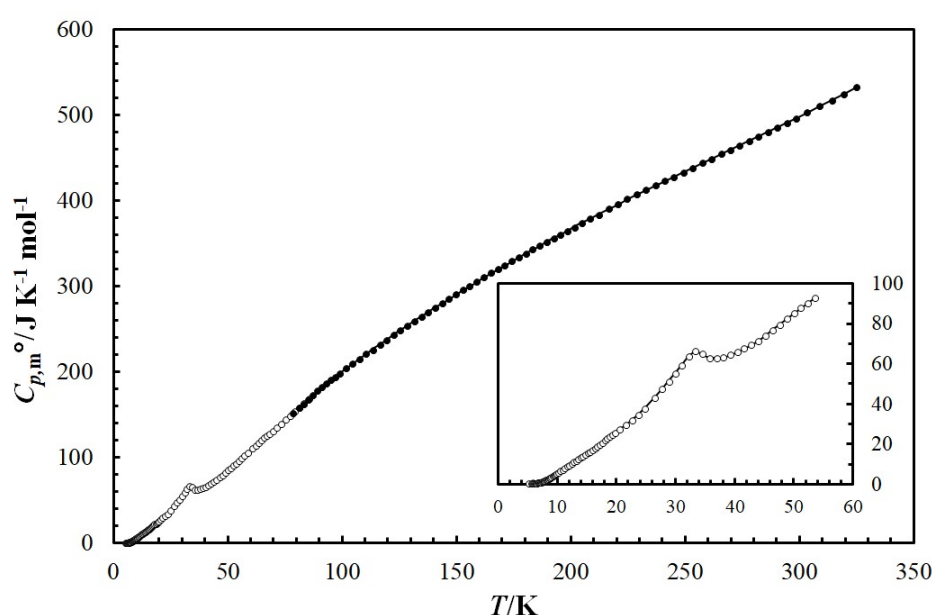


**Figure 4.** Temperature dependence of isobaric heat capacity,  $C_{p,m}^\circ(T)/\text{J}\cdot\text{K}^{-1}\cdot\text{mol}^{-1}$ , of mandarinoite (cr) in the temperature range from  $T = 5.2 \text{ K}$  to  $324.8 \text{ K}$ . Experimental data obtained using liquid helium ( $T = 5.2 \text{ K}$  to  $85.4 \text{ K}$ ) are shown as open circles ( $\circ$ ) and experimental data using liquid nitrogen ( $T = 78.7 \text{ K}$  to  $324.8 \text{ K}$ ) are shown as solid circles ( $\bullet$ ). The solid curve corresponds to extrapolation of experimental data using Equation (10).

In order to extrapolate the heat-capacity behavior down to  $T = 0 \text{ K}$ , we used the equation  $C_{p,m}^\circ = A \cdot T^n$ , where  $A$  and  $n$  are fit parameters that were determined using experimental data between  $T = 5.5$  and  $6.5 \text{ K}$  (polynomial Equation (9), see below). In logarithmic form we obtain for the respective compounds:

$$\ln \frac{C_{p,m}^\circ}{\text{J}\cdot\text{K}^{-1}\cdot\text{mol}^{-1}} = 1.9633 \ln \left( \frac{T}{\text{K}} \right) - 4.3051, \text{ with an error less than } 0.73\%. \quad (9)$$

In standard notation one has  $C_{p,m}^\circ = 0.0135 \cdot T^{1.9633}$ .

The heat capacity ( $C_{p,m}^\circ(T)$ ) data for the  $\text{Fe}_2(\text{SeO}_3)_3 \cdot 5\text{H}_2\text{O}(\text{cr})$  were fit over the five different temperature ranges (from  $T = 5.3$  to  $9 \text{ K}$ , from  $T = 10$  to  $21 \text{ K}$ , from  $T = 22$  to  $32 \text{ K}$ , from  $T = 33$  to  $64 \text{ K}$



and from  $T = 65$  to  $325$  K) by the method of nonlinear least squares, using the following polynomial equation [24]:

$$\frac{C_{p,m}^o}{\text{J}\cdot\text{K}^{-1}\cdot\text{mol}^{-1}} = k_0 + k_1\left(\frac{T}{\text{K}}\right)^{-3} + k_2\left(\frac{T}{\text{K}}\right)^{-2} + k_3\left(\frac{T}{\text{K}}\right)^{-0.5} + k_4\left(\frac{T}{\text{K}}\right) + k_5\left(\frac{T}{\text{K}}\right)^2 + k_6\left(\frac{T}{\text{K}}\right)^3. \quad (10)$$

The final best-fit values of the polynomial coefficients  $k_i$  are presented in the Supplementary Materials (see Table S4). The difference between the experimental  $C_{p,m}^o$  data and the fitted  $C_{p,m}^o$  values is presented in Figure S5.

## 4. Discussion

### 4.1. The Gibbs Energy of Formation

The standard molar entropy at  $298.15$  K,  $S_m^o$ , for the ferric selenite hydrate  $\text{Fe}_2(\text{SeO}_3)_3\cdot 5\text{H}_2\text{O}(\text{cr})$  was calculated from the smoothed  $C_{p,m}^o$  data by numerically solving the integral

$$S_m^o - S^{T=0\text{K}} = \int_0^{298.15} \frac{C_{p,m}^o}{T} dT, \quad (11)$$

assuming  $S^{T=0\text{K}} = 0$ . We obtain  $520.1 \pm 1.1 \text{ J}\cdot\text{K}^{-1}\cdot\text{mol}^{-1}$ . The expanded uncertainties for  $S$  are given at the 0.95 confidence level ( $k \approx 2$ ).

For the calculation of the entropy of formation at  $T = 298.15$  K,  $\Delta_f S_m^o$ , of mandarinoite(cr), its respective measured  $S_m^o$  value, together with the data in Table 4, was used. We obtain with the uncertainty given as two standard deviations of the mean:

$$\Delta_f S_m^o(\text{Fe}_2(\text{SeO}_3)_3\cdot 5\text{H}_2\text{O}, \text{cr}) = -1756.7 \pm 1.1 \text{ J}\cdot\text{K}^{-1}\cdot\text{mol}^{-1}.$$

**Table 4.** Standard entropies of elemental substances at  $T = 298$  K and  $p = 0.1$  MPa [22].

Substance	$S_m^o/\text{J}\cdot\text{K}^{-1}\cdot\text{mol}^{-1}$
Fe, cr	30.04
Se, cr	42.442
O <sub>2</sub> , gas	205.138
H <sub>2</sub> , gas	130.684

Finally, the standard molar Gibbs free energy of formation,  $\Delta_f G_m^o$ , for the ferric selenite hydrate  $\text{Fe}_2(\text{SeO}_3)_3\cdot 5\text{H}_2\text{O}(\text{cr})$  at  $T = 298.15$  K and  $p = 0.1$  MPa can be calculated using the newly obtained values of  $\Delta_f S_m^o$  and  $\Delta_f H_m^o$ . We calculate with the uncertainty given as two standard deviations of the mean:

$$\Delta_f G_m^o(\text{Fe}_2(\text{SeO}_3)_3\cdot 5\text{H}_2\text{O}, \text{cr}) = -2600.8 \pm 5.4 \text{ kJ}\cdot\text{mol}^{-1}.$$

Table 5 lists smoothed  $C_{p,m}^o(T)$  values between  $T \rightarrow 0$  and  $320$  K as well as the values for  $S_m^o$  and the functions  $[H_m^o(T) - H_m^o(0)]$  and  $[\Phi_m^o(T) - \Phi_m^o(0)]$ .

**Table 5.** Standard molar thermodynamic functions of mandarinoite(cr) at  $p = 0.1$  MPa <sup>a</sup>.  
 $\Delta_0^T \Phi_m^o(T) = \Delta_0^T S_m^o(T) - \Delta_0^T H_m^o(T)/T$ .

$T/K$	$C_{p,m}^o(T)$ $J \cdot K^{-1} \cdot mol^{-1}$	$\Delta_0^T H_m^o(T)$ $kJ \cdot mol^{-1}$	$\Delta_0^T S_m^o(T)$ $J \cdot K^{-1} \cdot mol^{-1}$	$\Delta_0^T \Phi_m^o(T)$ $J \cdot K^{-1} \cdot mol^{-1}$
[0]	[0]	[0]	[0]	[0]
5	0.319	0.0005	0.162	0.055
10	5.381	0.010	1.226	0.263
15	15.07	0.061	5.259	1.200
20	26.09	0.163	11.05	2.904
25	38.44	0.323	18.14	5.227
30	55.55	0.557	26.64	8.064
35	63.83	0.872	36.31	11.41
40	64.91	1.189	44.78	15.06
45	73.68	1.533	52.88	18.81
50	84.70	1.929	61.21	22.63
70	131.4	4.093	97.17	38.70
90	178.7	7.199	136.0	55.96
110	220.0	11.20	175.9	74.14
130	256.6	15.97	215.7	92.86
150	290.5	21.44	254.8	111.9
170	322.5	27.57	293.1	130.9
190	352.7	34.33	330.7	150.0
210	381.2	41.67	367.4	169.0
230	408.3	49.57	403.3	187.8
250	434.2	57.99	438.4	206.4
270	459.6	66.93	472.8	224.9
273.15	463.6	68.39	478.1	227.8
290	485.1	76.38	506.5	243.1
298.15	495.7	80.37	520.1	250.5
310	511.6	86.34	539.7	261.2
320	525.5	91.53	556.2	270.2

<sup>a</sup> Standard uncertainties,  $u$ , are  $u(T) = 0.05$  K,  $u(p) = 0.001$  MPa. The combined expanded uncertainties,  $U_{c,r}$  are  $U_{c,r}(C_{p,m}^o(T)) = 0.02$  for  $T < 15$  K, 0.005 from  $T = 15$  to 40 K, 0.002 between  $T = 40$  K and  $T = 330$  K,  $U_{c,r}(\Delta_0^T S_m^o(T)) = 0.022$  for  $T < 15$  K, 0.0055 between  $T = 15$  K and  $T = 40$  K, 0.0022 between  $T = 40$  K and  $T = 330$  K,  $U_{c,r}(\Delta_0^T H_m^o(T)) = 0.022$  for  $T < 15$  K, 0.0055 between  $T = 15$  K and  $T = 40$  K, 0.0022 between  $T = 40$  K and  $T = 330$  K,  $U_{c,r}(\Delta_0^T \Phi_m^o(T)) = 0.022$  for  $T < 15$  K, 0.0055 between  $T = 15$  K and  $T = 40$  K, 0.0022 between  $T = 40$  K and  $T = 330$  K (0.95 level of confidence).

#### 4.2. Stability of Mandarinoite in the Oxidation Zone

These results motivate a re-evaluation of the conditions under which ferric selenite could replace iron selenides, and Se-bearing sulfides in the oxidation zones of sulfide ore deposits or upon weathering of technologic waste. Special attention should be given to a substantiation of the thermodynamic approach for the modeling of mineral-forming processes in near-surface conditions.

The obtained value of  ${}_fG_m^o$  for  $Fe_2(SeO_3)_3 \cdot 5H_2O$  was used to calculate the Eh–pH diagram of the Fe–Se– $H_2O$  system. Previously, this diagram was calculated [1,2,14] on the basis of data on solubility obtained by Rai et al. [13] and recommended in [10].

Using the obtained value of  $\Delta_f G_m^o(Fe_2(SeO_3)_3 \cdot 5H_2O, cr) = -2600.8 \pm 5.4$   $kJ \cdot mol^{-1}$  and the literature data [22], namely  $\Delta_f G_m^o(298$  K,  $Fe^{3+}, aq) = -4.7$   $kJ \cdot mol^{-1}$ ,  $\Delta_f G_m^o(298$  K,  $SeO_3^{2-}, aq) = -369.8$   $kJ \cdot mol^{-1}$ ,  $\Delta_f G_m^o(298$  K,  $H_2O, liq) = -237.129$   $kJ \cdot mol^{-1}$ , the solubility product ( $SP$ ) of  $Fe_2(SeO_3)_3 \cdot 5H_2O(cr)$  at  $T = 298.15$  K has been calculated:  $\log_{10} SP(298$  K) =  $-51.90$ . Calculation of the Eh–pH diagram was by means of the software Geochemist’s Workbench, University of Illinois, USA (GMB 9.0). The calculation was predated by the introduction of new data for  $Fe_2(SeO_3)_3 \cdot 5H_2O$  into the database and the specification of some constants. The activity coefficients are calculated from the Debye–Hückel equation. Eh–pH diagrams of Fe–Se– $H_2O$  systems have been constructed for the average contents of these elements in acidic waters of the oxidation zones of sulfide deposits [1,2,14].

Finally, the Eh-pH plot of the Fe–Se–H<sub>2</sub>O system is shown in Figure 5. This system attracts interest because it allows the estimation of the physical-chemical parameters of the formation of hydrous ferric selenite, mandarinoite. The diagram contains a native selenium stability field, and FeSe (achavalite), FeSe<sub>2</sub> (ferroselite), FeO (wüstite), FeFe<sub>2</sub>O<sub>4</sub> (magnetite), Fe<sub>2</sub>O<sub>3</sub> (hematite), and ferric selenite (mandarinoite) stability fields. As follows from this diagram, Fe<sub>2</sub>(SeO<sub>3</sub>)<sub>3</sub>·5H<sub>2</sub>O is the stable phase at the temperature fluctuations corresponding to the environmental conditions in the acid to neutral areas at a high positive Eh.

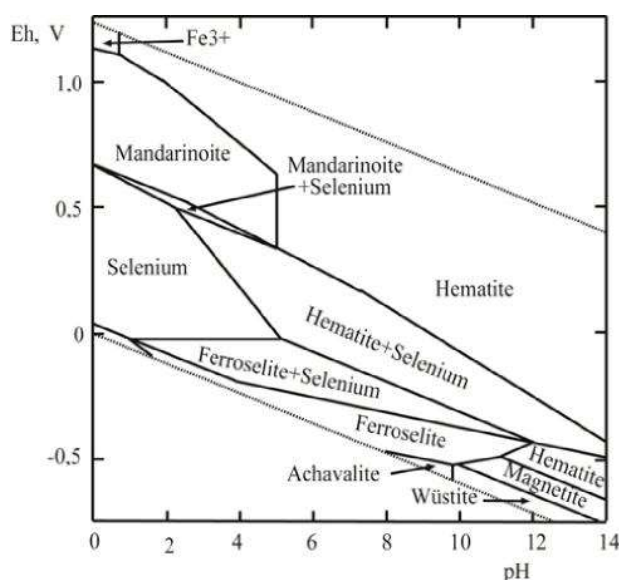


**Figure 5.** Eh-pH diagram of Fe-Se-H<sub>2</sub>O system at 25 °C and the activities of the components:  $a_{\Sigma\text{Se}} = 10^{-5}$ ,  $a_{\Sigma\text{Fe}} = 10^{-2}$ .

It is interesting to compare the conditions of copper and iron selenite formation in the oxidation zone of selenium-containing sulfide ores because copper (like iron) is a widespread element in primary ores. For this purpose, an Eh-pH diagram of the Fe-Cu-Se-CO<sub>2</sub>-H<sub>2</sub>O system has been constructed to obtain the thermodynamic properties of chalcocite [4] and the average contents of these elements in acidic waters of the oxidation zones of sulfide deposits (Figure 6). This system attracts interest because it allows the estimation of the physical-chemical parameters of the formation of hydrous Fe and Cu selenites (mandarinoite and chalcocite), which are associated in the oxidation zones of some selenium-bearing deposits (e.g., Virgen de Surumi mine [6], El Dragón mine [25], Baccu Locci Mine [26]). As can be seen, copper selenides and oxides (klockmannite CuSe, krut'aite CuSe<sub>2</sub>, umangite, Cu<sub>3</sub>Se<sub>2</sub>, cuprite Cu<sub>2</sub>O, and tenorite CuO) are largely stable at lower concentrations of copper and selenium. Under oxidative conditions, a narrow field of chalcocite appears in the mandarinoite stability field (Figure 6).

As shown previously, the stability of hydrous selenites of cobalt (cobaltomenite CoSeO<sub>3</sub>·2H<sub>2</sub>O) [3], nickel (ahlfeldite, NiSeO<sub>3</sub>·2H<sub>2</sub>O) [3], zinc (ZnSeO<sub>3</sub>·2H<sub>2</sub>O and ZnSeO<sub>3</sub>·H<sub>2</sub>O) [5,27] and cadmium (CdSeO<sub>3</sub>·H<sub>2</sub>O) [5,28] correspond to the conditions of mandarinoite formation, with the only difference that mandarinoite crystallized in a more wide range of pH values. It should be noted that zinc and cadmium selenites have not yet been found in the oxidation zone of sulfide and selenide ores because, in our opinion, diagnostics are partly hampered: Zn and Cd (in contrast to Cu, Co, Ni, and Fe) are not chromophores and therefore their salts are colorless or white.

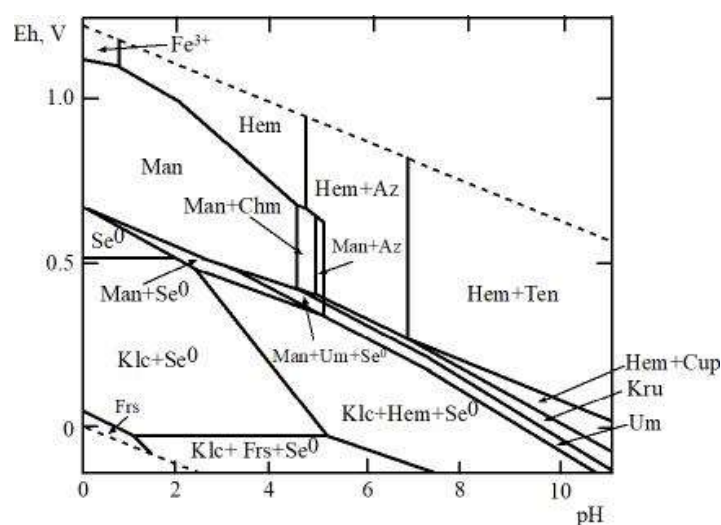


**Figure 6.** Eh-pH diagram of Fe-Cu-Se-CO<sub>2</sub>-H<sub>2</sub>O system at 25 °C and the activities of the components:  $a_{\Sigma\text{Se}} = 10^{-5}$ ,  $a_{\Sigma\text{Fe}} = 10^{-2}$ ,  $a_{\Sigma\text{Cu}} = 10^{-2}$ ,  $a_{\Sigma\text{CO}_2} = 10^{-3}$ . Notes: Se<sup>0</sup>—native selenium, Man—mandarinoite, Chm—chalcomenite, Hem—hematite, Frs—ferroselite, Klc—klockmannite, Kru—krut’aitite, Um—umangite, Cup—cuprite, Ten—tenorite.

## 5. Conclusions

The obtained thermodynamic constants of mandarinoite can be used to determine the conditions of selenium and iron behavior in the near-surface and surface environment. The distribution of these elements in soil and water and their mobility can be quantitatively explained by variations in the redox potential and the acidity-basicity of the mineral-forming medium. In general, these parameters determine the migration ability of selenium compounds and their precipitation in the form of various solid phases.

**Supplementary Materials:** The following are available online at <http://www.mdpi.com/2076-3263/8/11/391/s1>, **Figure S1:** Deviation of the  $C_{p,m}^{\circ}(T)/\text{J}\cdot\text{K}^{-1}\cdot\text{mol}^{-1}$  values for benzoic acid from literature data presented in [1]. **Figure S2:** Deviation of the  $C_{p,m}^{\circ}(T)/\text{J}\cdot\text{K}^{-1}\cdot\text{mol}^{-1}$  values for synthetic sapphire from literature data presented in [2]. **Figure S5:** Deviation of the raw experimental  $C_{p,m}^{\circ}(T)$  data for  $\text{Fe}_2(\text{SeO}_3)_3\cdot 5\text{H}_2\text{O}(\text{cr})$  from the polynomial fit in % (Equation (9) and Table S4). **Table S3:** Raw  $C_{p,m}^{\circ}$  ( $\text{J}\cdot\text{K}^{-1}\cdot\text{mol}^{-1}$ ) data for the  $\text{Fe}_2(\text{SeO}_3)_3\cdot 5\text{H}_2\text{O}(\text{cr})$ ,  $M = 582.669 \text{ g}\cdot\text{mol}^{-1}$  at  $p = 0.1 \text{ MPa}$ . **Table S4:** Best-fit coefficients for use in the  $C_{p,m}^{\circ}(T)$  polynomial of Equation (9) for  $\text{Fe}_2(\text{SeO}_3)_3\cdot 5\text{H}_2\text{O}(\text{cr})$  for the five temperature intervals.

**Author Contributions:** Conceptualization, methodology, visualization, and writing—review and editing, M.V.C. and V.G.K.; conceiving and designing the calorimetric investigations, M.I.L. and E.V.S.; preparation of the synthetic analogue of mandarinoite, B.L. and A.H.; writing—original draft preparation, M.I.L. and A.H. All authors have read and approved the final manuscript.

**Funding:** This research was funded by the Ministry of Education and Science of Russia grant 4.5510.2017/8.9 to MIL and EVS.

**Acknowledgments:** We wish to thank two anonymous reviewers for their thorough reviews and discussions which significantly improved this work. Research was carried out on the equipment of the Collective Usage Center “New Materials and Energy Saving Technologies” of Lobachevsky State University of Nizhni Novgorod and the Resource Center Geomodel, Centre for X-ray Diffraction Studies (Saint-Petersburg State University).

**Conflicts of Interest:** The authors declare no conflict of interest. The funders had no role in the design of the study; in the collection, analyses, or interpretation of data; in the writing of the manuscript, or in the decision to publish the results.

## References

1. Charykova, M.V.; Krivovichev, V.G. Mineral systems and the thermodynamics of selenites and selenates in the oxidation zone of sulfide ores—A review. *Mineral. Petrol.* **2017**, *111*, 121–134. [CrossRef]

2. Krivovichev, V.G.; Charykova, M.V.; Vishnevsky, A.V. The Thermodynamics of Selenium Minerals in Near-Surface Environments. *Minerals* **2017**, *7*, 188. [[CrossRef](#)]
3. Charykova, M.V.; Krivovichev, V.G.; Lelet, M.I.; Yakovenko, O.S.; Suleimanov, E.V.; Depmeier, W.; Semenova, V.V.; Zorina, M.L. A calorimetric and thermodynamic investigation of the synthetic analogues of cobaltomenite,  $\text{CoSeO}_3 \cdot 2\text{H}_2\text{O}$ , and ahlfeldite,  $\text{NiSeO}_3 \cdot 2\text{H}_2\text{O}$ . *Am. Mineral.* **2014**, *99*, 742–748. [[CrossRef](#)]
4. Charykova, M.V.; Lelet, M.I.; Krivovichev, V.G.; Ivanova, N.M.; Suleimanov, E.V. A calorimetric and thermodynamic investigation of the synthetic analogue of chalcomenite,  $\text{CuSeO}_3 \cdot 2\text{H}_2\text{O}$ . *Eur. J. Mineral.* **2017**, *29*, 269–277. [[CrossRef](#)]
5. Lelet, M.I.; Charykova, M.V.; Krivovichev, V.G.; Efimenko, N.M.; Platonova, N.V.; Suleimanov, E.V. A Calorimetric and Thermodynamic Investigation of Zinc and Cadmium Hydrous Selenites. *J. Chem. Thermodyn.* **2017**, *115*, 63–73. [[CrossRef](#)]
6. Dunn, P.J.; Pecker, D.R.; Sturman, B.D. Mandarinite—New ferric-iron selenite from Bolivia. *Can. Mineral.* **1978**, *16*, 605–609.
7. Hawthorne, F.C. The crystal structure of mandarinite,  $\text{Fe}^{3+}_2\text{Se}_3\text{O}_9 \cdot 6\text{H}_2\text{O}$ . *Can. Mineral.* **1984**, *22*, 475–480.
8. Holzheid, A.; Charykova, M.V.; Krivovichev, V.G.; Ledwig, B.; Fokina, E.L.; Poroshina, K.L.; Platonova, N.V.; Gurzhiy, V.V. Thermal behavior of ferric selenite hydrates ( $\text{Fe}_2(\text{SeO}_3)_3 \cdot 3\text{H}_2\text{O}$ ,  $\text{Fe}_2(\text{SeO}_3)_3 \cdot 5\text{H}_2\text{O}$ ) and the water content in the natural ferric selenite mandarinite. *Chem. Erde* **2018**, *78*, 228–240. [[CrossRef](#)]
9. Séby, F.; Potin-Cautier, M.; Giffaut, E.; Borge, G.; Donard, O.F.X. A critical review of thermodynamic data for selenium species at 25 °C. *Chem. Geol.* **2001**, *171*, 173–194. [[CrossRef](#)]
10. Olin, A.; Nolang, B.; Osadchii, E.G.; Ohman, L.-O.; Rosen, E. *Chemical Thermodynamics of Selenium*; Elsevier: Amsterdam, The Netherlands, 2005; 851p.
11. Charykova, M.V.; Krivovichev, V.G.; Depmeier, W. Thermodynamics of arsenates, selenites and sulphates in oxidising zone of sulphides ore deposits. Part I: Thermodynamic properties at standard conditions. *Geol. Ore Depos.* **2010**, *52*, 759–770. [[CrossRef](#)]
12. Chukhlantsev, V.G.; Tomashevsky, G.P. The Solubility of Selenites of Certain Metals. *Zh. Anal. Khim.* **1957**, *12*, 296–301. (In Russian)
13. Rai, D.; Felmy, A.R.; Moore, D.A. The solubility product of crystalline ferric selenite hexahydrate and the complexation constant of  $\text{FeSeO}_3^+$ . *J. Sol. Chem.* **1995**, *24*, 735–752. [[CrossRef](#)]
14. Krivovichev, V.G.; Charykova, M.V.; Yakovenko, O.S.; Depmeier, W. Thermodynamics of Arsenates, Selenites, and Sulfates in the Oxidation Zone of Sulfide Ores. IV. Eh–pH Diagrams of the Me–Se–H<sub>2</sub>O Systems (Me = Co, Ni, Fe, Cu, Zn, Pb) at 25 °C. *Geol. Ore Depos.* **2011**, *53*, 514–527. [[CrossRef](#)]
15. Giester, G.; Pertlik, F.; Brandstätter, F. A revision of the formula  $\text{Fe}_2(\text{SeO}_3)_3 \cdot 6\text{H}_2\text{O}$  to  $\text{Fe}_2(\text{SeO}_3)_3 \cdot 3\text{H}_2\text{O}$ . *Mater. Res. Bull.* **1996**, *31*, 1189–1193. [[CrossRef](#)]
16. Rai, D.; Mattigod, S.; Moore, D. Characterization of  $\text{Fe}_2(\text{SeO}_3)_3 \cdot 6\text{H}_2\text{O}$ , a new synthetic ferric selenite. *Mater Res. Bull.* **1988**, *23*, 1621. [[CrossRef](#)]
17. Furukawa, G.T.; McCoskey, R.E.; King, G.J. Calorimetric Properties of Benzoic Acid from 0 to 410. *J. Res. Natl. Bur. Stand.* **1951**, *47*, 256–261. [[CrossRef](#)]
18. Ditmars, D.A.; Ishihara, S.; Chang, S.S.; Bernstein, G. Enthalpy and Heat-Capacity Standard Reference Material: Synthetic Sapphire ( $\alpha\text{-Al}_2\text{O}_3$ ) from 10 to 2250 K. *J. Res. Natl. Bur. Stand.* **1982**, *87*, 159–163. [[CrossRef](#)]
19. Varushchenko, R.M.; Druzhinina, A.I.; Sorkin, E.L. Low-temperature heat capacity of 1-bromoperfluorooctane. *J. Chem. Thermodyn.* **1997**, *29*, 623–637. [[CrossRef](#)]
20. Lelet, M.I.; Sharkov, V.V.; Nurgaliev, I.F.; Suleymanov, Y.V. A new hardware solution in reaction calorimetry. *Vestn. Nizhny Novgorod State Univ.* **2011**, *3*, 97–101.
21. Glushko, V.P. (Ed.) *Thermal Constants of Compounds*; Academy of Science, SSSR: Moscow, Russia, 1965–1982; Volume 1–10. (In Russian)
22. Melnikov, P.; Nascimento, V.A.; Arkhangelsky, I.V.; Zaroni Consolo, L.Z.; de Oliveira, L.C.S. Thermal decomposition mechanism of iron(III) nitrate and characterization of intermediate products by computerized modeling. *J. Therm. Anal. Cal.* **2014**, *115*, 145–151. [[CrossRef](#)]
23. Wagman, D.D.; Evans, W.H.; Parker, V.B.; Schumm, R.H.; Halow, I.; Bailey, S.M.; Churney, K.L.; Nuttall, R.L. The NBS tables of chemical thermodynamic properties: Selected values for inorganic and C1 and C2 organic substances in (SI) units. *J. Phys. Chem. Ref. Data* **1982**, *11* (Suppl. 2), 1–392.

24. Dachs, E.; Geiger, C.A. Heat capacities and vibrational entropies of mixing of pyrope-grossular ( $\text{Mg}_3\text{Al}_2\text{Si}_3\text{O}_{12}$ - $\text{Ca}_3\text{Al}_2\text{Si}_3\text{O}_{12}$ ) garnet solid solutions: A low temperature calorimetric and thermodynamic investigation. *Am. Mineral.* **2006**, *91*, 894–906. [[CrossRef](#)]
25. Grundmann, G.; Förster, H.-J. Origin of the El Dragón Selenium Mineralization, Quijarro Province, Potosí, Bolivia. *Minerals* **2017**, *7*, 68. [[CrossRef](#)]
26. Campostrini, I.; Gramaccioli, C.M. Selenium-rich secondary minerals from the Bacchu Locci mine (Sardinia, Italy). *Neues Jahrb. Mineral. Abh.* **2001**, *177*, 37–59. [[CrossRef](#)]
27. Charykova, M.V.; Krivovichev, V.G.; Ivanova, N.M.; Semenova, V.V. Thermodynamics of Arsenates, Selenites, and Sulfates in the Oxidation Zone of Sulfide Ores. XI. Solubility of Synthetic Chalcocite Analog and Zinc Selenite at 25 °C. *Geol. Ore Depos.* **2015**, *57*, 691–698. [[CrossRef](#)]
28. Charykova, M.V.; Vishnevsky, A.V.; Krivovichev, V.G.; Fokina, E.L.; Ivanova, N.M.; Platonova, N.V.; Semenova, V.V. Thermodynamics of Arsenates, Selenites and Sulfates in the Oxidation Zone of Sulfide Ores. XII. Mineral Equilibria in the Cd–Se–H<sub>2</sub>O System at 25 °C. *Geol. Ore Depos.* **2016**, *58*, 636–645. [[CrossRef](#)]



© 2018 by the authors. Licensee MDPI, Basel, Switzerland. This article is an open access article distributed under the terms and conditions of the Creative Commons Attribution (CC BY) license (<http://creativecommons.org/licenses/by/4.0/>).